AIMS Mathematics, 11(3): 8792–8811.
DOI: 10.3934/math.2026361
Received: 21 October 2025
Revised: 23 December 2025
Accepted: 06 January 2026
Published: 31 March 2026

https://www.aimspress.com/journal/Math

Research article

A Bayesian cure rate model using the Bell–Touchard distribution and Hamiltonian Monte Carlo methods

Manuel J. P. Barahona*, Yolanda M. Gómez and Diego I. Gallardo

Departamento de Estadística, Facultad de Ciencias, Universidad del Bío-Bío, Concepción, Chile

* **Correspondence:** Email: mpereira@ubiobio.cl; Tel: +56413111009.

Abstract: We proposed a novel cure rate model in which the number of competing causes follows a Bell–Touchard distribution. We derived its main mathematical properties and implemented Bayesian inference using the Hamiltonian Monte Carlo algorithm. A simulation study was conducted to assess the finite-sample performance of the estimators. The model's applicability was demonstrated using two real datasets: patients with melanoma and patients with cardiovascular disease. In the latter dataset, diabetic patients exhibited higher estimated cure and survival probabilities than non-diabetic individuals, potentially reflecting phenomena such as "reverse epidemiology" or intensified clinical management.

Keywords: Bell-Touchard distribution; long-term survival model; Hamiltonian Monte Carlo; reparameterization
Mathematics Subject Classification: 62F15, 62N01, 62N02, 62P10, 65C05

1. Introduction

With medical advances, an increasing number of cancer types now have treatments that allow patients to live as long as individuals without the disease. In this context, cure rate models have emerged as valuable tools for analysis. The pioneering works of [1] and [2] introduced the Bernoulli cure rate (Berncr) model by assuming the existence of two subpopulations: cured and susceptible individuals. This formulation is characterized by a Bernoulli-distributed latent variable M, where $M = 0$ denotes a cured individual and $M = 1$ a susceptible one. Subsequently, [3] proposed the Poisson cure rate (Pocr) model, in which the latent variable M represents the number of unobservable competing causes (e.g., carcinogenic cells in cancer studies) and is assumed to follow a Poisson distribution. The Pocr model has been widely adopted in the literature, partly because it is connected to proportional hazards models.

In recent years, a wide variety of *cure rate models* have been developed by specifying different

distributions for the number of *competing causes* M. This line of research has incorporated several discrete distributions, including the negative binomial [4], COM-Poisson [5], power series [6], Yule–Simon [7], polylogarithm [8], modified power series [9], zero-inflated power series [10], zero-modified geometric [11], zero-inflated Bernoulli [12], Nielsen [13], compound Poisson [14], mixtures within the PS (power series) class [14], generalized Poisson [15], Waring [16], mixtures of Poisson and Birnbaum–Saunders distributions [17], and further developments in zero-inflated power series models [18], among others.

Within this context, we propose the use of the Bell–Touchard (BT) distribution, recently introduced by [19], as a flexible choice for modeling the number of competing causes. The probability mass function (pmf) of the BT distribution is given by

$$P(M = m; \theta, \alpha) = \frac{e^{\alpha(1-e^{\theta})}\theta^m T_m(\alpha)}{m!}, \quad m = 0, 1, 2, \ldots, \tag{1.1}$$

for $\theta, \alpha > 0$, where $T_n(\alpha)$ denotes the Touchard polynomials, defined as:

$$T_n(\alpha) = e^{-\alpha} \sum_{k=0}^{\infty} \frac{k^n \alpha^k}{k!}.$$

These polynomials correspond to the n-th moment of the Poisson distribution. We write $M \sim \text{BT}(\theta, \alpha)$ when a random variable M follows the distribution in (1.1).

A key property of the BT distribution is its closed-form probability generating function (pgf), which is given by

$$G_M(s) = \mathbb{E}[s^M] = \exp\left\{\alpha\left(e^{s\theta} - e^{\theta}\right)\right\}, \quad |s| < 1. \tag{1.2}$$

This distribution presents several advantages to be considered in a cure rate model framework:

i. **Analytical tractability:** The closed-form pgf facilitates theoretical derivations, particularly in the cure rate setting, where the population survival function directly depends on the pgf.
ii. **Simple expression for the cure fraction:** The probability of no competing causes is given by $P(M = 0; \theta, \alpha) = \exp\{\alpha(1 - e^{\theta})\}$, which enables a direct reparameterization of the model in terms of the cure fraction, which allows the covariates to be introduced directly through this term, facilitating the comparison between different models.
iii. **Connection to known models:** Setting $\alpha = 1$ yields the (shifted) Bell distribution, introduced in [20] in the context of cure rate models (named the Bellcr model). To the best of our knowledge, the more general BT distribution has not yet been explored for modeling the number of competing causes. In addition, we are also not aware of any model in the literature that contains the Bellcr model as a particular case.

Beyond its mathematical convenience, the proposed cure rate model based on the BT distribution is motivated by real-world applications in medical research. For instance, melanoma is a type of cancer in which long-term survivors are frequently observed due to effective treatment strategies, making cure rate models particularly suitable. To illustrate this, we analyze the melanoma dataset available in the `timereg` package in R, which has been widely used in the survival analysis literature.

We also consider an application in cardiovascular disease, specifically for patients with ST-elevation myocardial infarction (STEMI). In this context, the prognostic significance of apelin-12

was examined in a prospective observational study with stratification by renal function [21, 22]. Applying cure rate models in this scenario may reveal heterogeneity in survival patterns and cured fractions across different patient subgroups. Together, these case studies from oncology and cardiology demonstrate the flexibility and practical relevance of the proposed Bell–Touchard cure rate (BTcr) model.

In addition, the literature on the use of Bayesian inference within the context of cure fraction models is limited. [23] and [24] discussed Bayesian inference in the negative binomial cure rate model, whereas [25] did the same for the Conway-Maxwell-Poisson cure rate model. [26] introduced a new approach for cure rate models, called destructive models, and discussed Bayesian inference. [27] discussed this kind of inference in the Poisson-inverse-Gaussian cure rate model, [28] did the same in the negative binomial cure rate model, but considered different activation schemes for the concurrent causes (not only the minimum, which is the most used in the literature and which we will present later), whereas [16] introduced the Waring cure rate model and performed Bayesian inference for the model. In all cases, the methods for drawing values from the posterior distributions used the Metropolis-Hastings (MH) algorithm. In the literature, in the context of cure rate models, we find only the work of [15], used the Hamiltonian Monte Carlo (HMC) algorithm for Bayesian inference in the generalized Poisson cure rate model. Given this shortcoming, we believe it is crucial to compare the methods for simulating values from the posterior distribution using the MH and HMC algorithm in this context. In a broader Bayesian reliability context, recent works such as [29] and [30] emphasized the relevance of efficient Bayesian computational strategies for latent variable and lifetime models, further supporting the methodological focus adopted here. The rest of this paper is organized as follows. In Section 2.1, we present the formulation of the BTcr model and discuss its main properties. Section 2.2.1 describes the estimation procedures and Bayesian inference methods. Section 3.1 provides a simulation study to evaluate the finite-sample performance of the estimators. In Section 3.2, we illustrate the model's applicability using two real datasets: melanoma data from the `timereg` package and the STEMI dataset from the apelin-12 observational study. Finally, Section 4 summarizes our findings and discusses potential future research directions.

2. Materials and methods

2.1. The model

Let M be an unobserved random variable representing the initial number of competing causes associated with the occurrence of a specific event of interest. In this proposal and for the first time in the literature, we assume that $M \sim \text{BT}(\alpha, \theta)$.

The standard formulation in this context follows the competing risks framework. Specifically, we assume that $W_1, W_2, \ldots$ denote the times until a detectable cancer arises from each carcinogenic cell. These times are assumed to be conditionally independent and identically distributed (i.i.d.), each following a common survival function $S(\cdot; \boldsymbol{\xi})$, where $\boldsymbol{\xi}$ is a vector of model parameters. The survival function is assumed to be proper, i.e., $S(\infty; \boldsymbol{\xi}) = 0$. Furthermore, the sequence $\{W_j\}_{j\geq 1}$ is assumed to be independent of M.

To account for the possibility of a cured individual (i.e., one who will never experience the event of interest), we define a latent variable W_0 such that $P(W_0 = \infty) = 1$. The observed time-to-event variable

T is then defined as

$$T = \min(W_0, W_1, \ldots, W_M),$$

which implies that $T = \infty$ if $M = 0$ (indicating a cured individual), and $T = \min(W_1, \ldots, W_M) < \infty$ if $M \geq 1$ (indicating a susceptible individual).

Following Theorem 2 in [4] (see also [31]), the population survival function of the proposed Bell–Touchard cure rate (BTcr) model is given by the composition of the pgf of the BT distribution with the survival function $S(\cdot; \boldsymbol{\xi})$:

$$S_{\text{pop}}(t; \theta, \alpha, \boldsymbol{\xi}) = P(T > t; \theta, \alpha, \boldsymbol{\xi}) = G(S(t; \boldsymbol{\xi}); \theta, \alpha) = \exp\left\{\alpha\left[e^{S(t;\boldsymbol{\xi})\theta} - e^{\theta}\right]\right\}. \tag{2.1}$$

The cure fraction (i.e., the long-term survival probability) is then obtained as

$$p = \lim_{t\to\infty} S_{\text{pop}}(t; \theta, \alpha, \boldsymbol{\xi}) = \exp\left\{\alpha(1 - e^{\theta})\right\} = P(M = 0; \theta, \alpha).$$

The corresponding population-level probability density function (pdf) and hazard function are derived as:

$$f_{\text{pop}}(t; \theta, \alpha, \boldsymbol{\xi}) = S_{\text{pop}}(t; \theta, \alpha, \boldsymbol{\xi}) \cdot \alpha\theta f(t; \boldsymbol{\xi}) \cdot e^{S(t;\boldsymbol{\xi})\theta},$$
$$\text{and} \quad h_{\text{pop}}(t; \theta, \alpha, \boldsymbol{\xi}) = \alpha\theta f(t; \boldsymbol{\xi}) \cdot e^{S(t;\boldsymbol{\xi})\theta},$$

where $f(t; \boldsymbol{\xi})$ is the baseline pdf corresponding to the survival function $S(t; \boldsymbol{\xi})$.

To account for heterogeneity among individuals, we reparameterize the model in terms of the cure fraction p, using the relation

$$p = \exp\left\{\alpha(1 - e^{\theta})\right\} \quad \Leftrightarrow \quad \theta = \log\left(1 - \frac{\log(p)}{\alpha}\right).$$

This reparameterization allows direct modeling of the cure fraction and facilitates its interpretation in regression settings.

For a sample of size n, let the covariates associated with the i-th individual be denoted by the vector $\mathbf{x}_i = (1, x_{1i}, \ldots, x_{ri})^{\top}$, where the symbol "$\top$" denotes transposition. The individual-specific cure rate p_i is linked to the covariates via a regression model of the form

$$p_i = p_i(\mathbf{x}_i, \boldsymbol{\beta}) = G(\mathbf{x}_i^{\top}\boldsymbol{\beta}), \tag{2.2}$$

where $G : \mathbb{R} \to (0, 1)$ is a known link function, and $\boldsymbol{\beta} = (\beta_0, \beta_1, \ldots, \beta_r)^{\top}$ is a vector of regression coefficients. A common choice is the logit link:

$$G(u) = \text{logit}^{-1}(u) = \frac{e^u}{1 + e^u} \Leftrightarrow G^{-1}(u) = \text{logit}(u) = \log\left(\frac{u}{1 - u}\right).$$

This formulation allows covariate-dependent modeling of the cure fraction, providing a flexible framework for analyzing heterogeneous populations in medical and epidemiological studies.

Remark 1. For the BTcr model, the survival function with the reparametrization is given by

$$S_{\text{pop}}(t; p, \alpha, \boldsymbol{\xi}) = \exp\left(\alpha\left(\exp\left(S(t; \boldsymbol{\xi}) \ln\left(1 - \frac{\ln(p)}{\alpha}\right)\right) - \left(1 - \frac{\ln(p)}{\alpha}\right)\right)\right)$$

$$= 1 - p + p \times \underbrace{\frac{\exp\left(\alpha\left(\exp\left(S(t;\boldsymbol{\xi})\ln\left(1-\frac{\ln(p)}{\alpha}\right)\right)-\left(1-\frac{\ln(p)}{\alpha}\right)\right)\right)}{p}}_{S_{sus}(t;p,\alpha,\boldsymbol{\xi})},$$

where $p = p(\mathbf{x}, \boldsymbol{\beta})$ is the cure rate depending on the observed covariates. In other words, $S_{\text{pop}}(\cdot)$ can be written as a mixture model [2] with cure rate p and survival function for the susceptible individual $S_{sus}(\cdot)$. As stated in point 2 of Theorem 1 in [32], the model is not identifiable when $p(\mathbf{x}, \boldsymbol{\beta})$ is constant (i.e., when the covariate vector $\mathbf{x}$ consists only of the intercept term). Therefore, the first and most essential condition for ensuring the identifiability of the model is that $\mathbf{x}$ includes at least one additional covariate. Consider the definitions

$$\|p\|_{\mathbf{x}} = \sup\{p(\boldsymbol{x}, \boldsymbol{\beta}) : \mathbf{x} \in \mathcal{X}\} \quad \text{and} \quad \|S^*\| = \sup\{S_{\text{sus}}(t; p, \alpha, \boldsymbol{\xi})\}.$$

Since $\pi(\boldsymbol{x}, \boldsymbol{\beta}) = G(\boldsymbol{x}_i^\top \boldsymbol{\beta})$, with $G : \mathbb{R} \to (0, 1)$ being a monotone function, it follows that $\|\pi\|_{\mathbf{x}} = 1$. Moreover, as $S_{sus}(t; p, \alpha, \boldsymbol{\xi})$ is a decreasing function in terms of $S(t; \boldsymbol{\xi})$, we have

$$0 = \lim_{t\to\infty} S_{sus}(t; p, \alpha, \boldsymbol{\xi}) \leq S_{sus}(t; p, \alpha, \boldsymbol{\xi}) \leq \lim_{t\to 0} S_{sus}(t; p, \alpha, \boldsymbol{\xi}) = 1.$$

It follows that $S_{sus}(t; p, \alpha, \boldsymbol{\xi}) \in [0, 1]$ and consequently $\|S^*\| = 1$. According to point 1 of Theorem 1 in [32], the model is thus identifiable.

2.2. Bayesian inference for the BTcr model

In this section, we detail the estimation of the parameters of the BTcr model presented in Section 2.1 within a Bayesian framework. We also discuss the estimation procedures employed.

2.2.1. Bayesian approach

We consider a setting where lifetimes are subject to right censoring. Let Y_i denote the failure time and C_i the censoring time for the i-th subject, $i = 1, ..., n$. The observed data consist of $T_i = \min(Y_i, C_i)$ and the indicator $\delta_i = I(Y_i \leq C_i)$, where $\delta_i = 1$ if the event of interest is observed (failure) and $\delta_i = 0$ if the observation is censored. Under the assumption of non-informative censoring and with p_i defined as in (2.2), the likelihood function for the parameter vector $\boldsymbol{\psi}$ is given by

$$L(\boldsymbol{\psi}; \mathcal{D}) \propto \prod_{i=1}^{n} h_{pop}(t_i|\boldsymbol{\psi})^{\delta_i} S_{pop}(t_i|\boldsymbol{\psi}),$$

where $\boldsymbol{\psi}^\top = (\boldsymbol{\beta}^\top, \boldsymbol{\xi}^\top, \alpha)$ and $\mathcal{D} = \{(t_i, \delta_i, \boldsymbol{x}_i) : i = 1, ..., n\}$ represents the observed data. Specifically for the BTcr model, the likelihood function can be expressed as

$$\begin{aligned} L(\boldsymbol{\psi}; \mathcal{D}) &\propto \prod_{i=1}^{n} \left(\alpha\theta f(t_i; \boldsymbol{\xi}) e^{\theta S(t_i;\boldsymbol{\xi})}\right)^{\delta_i} \times \left(\exp\{\alpha[e^{\theta S(t_i;\boldsymbol{\xi})} - e^{\theta}]\}\right) \\ &\propto \prod_{i=1}^{n} \exp\left\{\alpha\left[\left(1-\frac{\log(p_i)}{\alpha}\right)^{S(t_i;\boldsymbol{\xi})} - \left(1-\frac{\log(p_i)}{\alpha}\right)\right]\right\} \times \end{aligned} \tag{2.3}$$

$$\left[\alpha \log\left(1 - \frac{\log(p_i)}{\alpha}\right) f(t_i;\boldsymbol{\xi}) \left(1 - \frac{\log(p_i)}{\alpha}\right)^{S(t_i;\boldsymbol{\xi})}\right]^{\delta_i}.$$

In this work, we assume the Weibull distribution for the time to event with parameterization given by $S(t,\boldsymbol{\xi}) = e^{-e^{\lambda}t^{\kappa}}$ and $f(t,\boldsymbol{\xi}) = e^{\lambda}\kappa t^{\kappa-1}e^{-e^{\lambda}t^{\kappa}}$. Therefore, the log-likelihood function becomes

$$l(\boldsymbol{\psi};\mathcal{D}) \propto \sum_{i=1}^{n} \delta_i \Bigg[\log(\alpha) + \log\left(\log\left(1 - \frac{\log(p_i)}{\alpha}\right)\right) + \lambda + \log(kt_i^{\kappa-1}) - e^{\lambda}t_i^{\kappa} + e^{-e^{\lambda}t_i^{\kappa}} \log\left(1 - \frac{\log(p_i)}{\alpha}\right) + \alpha\left\{\left(1 - \frac{\log(p_i)}{\alpha}\right)^{e^{-e^{\lambda}t_i^{\kappa}}} - \left(1 - \frac{\log(p_i)}{\alpha}\right)\right\}\Bigg].$$

To implement the Bayesian approach, we specify prior distributions for the model parameters. We assume prior independence among the parameters, so that $\pi(\boldsymbol{\psi}) = \pi(\boldsymbol{\beta})\pi(\boldsymbol{\xi})\pi(\alpha)$. Additionally, we consider prior independence within the elements of $\boldsymbol{\beta}$ and within $\boldsymbol{\xi}$. We assign normal prior distributions to λ and β_j for $j = 1, .., r$, and gamma prior distributions to k and α. Therefore, using this prior configuration and the likelihood in equation (2.3), the posterior distribution of $\boldsymbol{\psi}$ is given by

$$\pi(\boldsymbol{\psi}|\mathcal{D}) \propto L(\boldsymbol{\psi};\mathcal{D})\pi(\boldsymbol{\psi}).$$

Since the posterior distribution $\pi(\boldsymbol{\psi}|\mathcal{D})$ is analytically intractable, we employ advanced computational methods to approximate it. Specifically, we utilize the HMC method as well as a custom Metropolis-Hastings (MH) algorithm, both implemented via the `rstan` package.

The HMC method is an advanced Markov chain Monte Carlo (MCMC) algorithm that leverages gradient information of the target distribution to generate efficient proposal steps, reducing autocorrelation between samples [33]. By introducing auxiliary momentum variables $\boldsymbol{r}$, we define a Hamiltonian function

$$H(\boldsymbol{\psi},\boldsymbol{r}) = -\log(\pi(\boldsymbol{\psi}|\mathcal{D})) + \frac{1}{2}\boldsymbol{r}^T\boldsymbol{M}^{-1}\boldsymbol{r},$$

where $\boldsymbol{M}$ is a mass matrix. The joint distribution $\pi(\boldsymbol{\psi},\boldsymbol{r}|\mathcal{D})$ is then explored using Hamiltonian dynamics, allowing the sampler to traverse the parameter space more effectively than traditional MCMC methods.

2.2.2. Predictive model comparison

We compare models by expected log pointwise predictive density estimated with Pareto-smoothed importance sampling (PSIS-LOO) [34, 35]. Let $\ell_i(\psi) = \log p(y_i \mid \psi)$ and $\{\psi^{(s)}\}_{s=1}^{S}$ are the posterior draws. PSIS yields smoothed importance weights to approximate $p(y_i \mid y_{-i})$ and pointwise contributions $\widehat{\mathrm{elpd}}_{\mathrm{loo},i} = \log \widehat{p}(y_i \mid y_{-i})$. We report $\widehat{\mathrm{elpd}}_{\mathrm{loo}} = \sum_{i=1}^{n} \widehat{\mathrm{elpd}}_{\mathrm{loo},i}$, $\mathrm{LOOIC} = -2\,\widehat{\mathrm{elpd}}_{\mathrm{loo}}$, and the effective number of parameters

$$p_{\mathrm{loo}} = \sum_{i=1}^{n} (\mathrm{lpd}_i - \widehat{\mathrm{elpd}}_{\mathrm{loo},i}), \quad \mathrm{lpd}_i = \log\Big(\tfrac{1}{S}\sum_{s=1}^{S} p(y_i \mid \psi^{(s)})\Big).$$

Standard errors (SEs) follow the variability of pointwise terms; for two models A, B, we report the difference and its SE:

$$\Delta\widehat{\text{elpd}} = \sum_{i=1}^{n}(\widehat{\text{elpd}}_{\text{loo},i}^{(A)} - \widehat{\text{elpd}}_{\text{loo},i}^{(B)}), \quad \text{se}_\Delta = \sqrt{n\,\widehat{\text{Var}}_i(\widehat{\text{elpd}}_{\text{loo},i}^{(A)} - \widehat{\text{elpd}}_{\text{loo},i}^{(B)})}.$$

We treat $|\Delta\widehat{\text{elpd}}| \lesssim \text{se}_\Delta$ as a practical tie. Computations use Stan pointwise log-likelihood (`log_lik`) and the `loo` package.

3. Results

3.1. Simulation study

The inferential performance of the BTcr model was evaluated through simulations that mimic four configurations, denoted m_1–m_4, defined by the pairs $(\alpha, \lambda) \in \{(2, -3), (2, -1), (0.8, -3), (0.8, -1)\}$ and fixed values $\boldsymbol{\beta} = (-0.5, 0.7, 1)^\top$ and $\kappa = 1.5$. For each configuration, $R = 1000$ data sets were generated with sample sizes $n \in \{200, 400, 1000\}$. Covariate vectors contained an intercept, a binary variable $x_1 \sim$ Bernoulli(0.6), and a continuous variable $x_2 \sim$ Uniform(0, 10). The cure fraction was defined as $p_i = \text{logit}^{-1}(x_i^\top \boldsymbol{\beta})$, yielding $\theta_i = \log(1 - \log(p_i)/\alpha)$; the number of competing causes followed $M_i \sim \text{BT}(\theta_i, \alpha)$. Each failure time corresponded to the minimum of M_i Weibull variables with parameters λ and κ, and administrative censoring was applied at $C = 30$.

Each replicate was analyzed with the HMC method in `Stan` (4000 iterations per chain, 50% warm-up) and with a random-walk Metropolis-Hastings (MH) algorithm run for 10,000 iterations, discarding the first 5000. For the MH sampler, we used independent Gaussian proposals for each parameter; the proposal variances were tuned in short pilot runs so that the acceptance probabilities stabilized in a moderate range (approximately 5–15%) and were then kept fixed across the 1000 replications. For every parameter ψ, we computed the mean absolute bias, the empirical standard error (SE), and the nominal 95% coverage probability (CP). Table 1 summarizes these indicators.

Table 1 exhibits clear differences between the two estimation algorithms. For the regression coefficients β_1, β_2, and β_3, both methods yield modest biases; however, when $n = 1000$, MH coverage drops below 90% (0.905, 0.883 and 0.910, respectively), whereas HMC remains close to the nominal 95%. The gap widens for the mixing parameter α: at $n = 200$, MH coverage is still adequate but decreases to 0.892 as the sample grows, and its mean bias is roughly twice that of HMC (0.873 versus 0.429). A similar pattern appears for λ; biases are small in absolute terms, yet the loss of coverage under MH indicates underestimated variances that do not improve with more data. Results for κ are less contrasted, but MH coverage again falls below the target when the acceptance rate drops under 3%.

HMC's stability stems from a more efficient exploration of the parameter space, producing consistently smaller empirical SEs. The trade-off is computational: HMC requires 20 to 90 seconds per replicate, compared with 3 to 10 seconds for MH; however, this advantage is offset by MH acceptance rates ranging from 13% to 5%, resulting in highly autocorrelated chains and inflated empirical variances. Overall, HMC delivers more accurate inference and coverage close to the nominal level across all scenarios. In contrast, MH is competitive only for small samples, at the cost of increasing inefficiency as information accumulates.

Table 1. Bias, empirical standard error (SE), and 95% coverage probability (CP) of the estimators obtained with both methods.

			$n = 200$			$n = 400$			$n = 1000$		
Model	Method	Param.	Bias	SE	CP	Bias	SE	CP	Bias	SE	CP
m_1	HMC	β_1	0.286	0.369	0.944	0.203	0.259	0.944	0.126	0.163	0.941
		β_2	0.251	0.304	0.943	0.178	0.214	0.947	0.108	0.135	0.951
		β_3	0.041	0.053	0.954	0.029	0.037	0.948	0.018	0.023	0.945
		α	0.243	2.035	0.992	0.338	1.988	0.994	0.429	1.877	0.998
		λ	0.192	0.273	0.964	0.138	0.209	0.976	0.100	0.155	0.975
		κ	0.085	0.113	0.949	0.060	0.082	0.971	0.040	0.055	0.948
	MH	β_1	0.293	0.357	0.933	0.210	0.246	0.924	0.133	0.154	0.905
		β_2	0.257	0.295	0.919	0.178	0.206	0.915	0.115	0.128	0.883
		β_3	0.042	0.052	0.940	0.030	0.036	0.923	0.019	0.022	0.910
		α	0.442	1.756	0.992	0.599	1.614	0.984	0.873	1.191	0.892
		λ	0.200	0.261	0.953	0.147	0.200	0.940	0.114	0.131	0.896
		κ	0.089	0.110	0.926	0.061	0.080	0.949	0.042	0.050	0.899
m_2	HMC	β_1	0.291	0.369	0.953	0.192	0.258	0.960	0.132	0.163	0.937
		β_2	0.248	0.305	0.939	0.164	0.214	0.953	0.104	0.135	0.947
		β_3	0.043	0.053	0.952	0.028	0.037	0.938	0.019	0.023	0.944
		α	0.229	2.004	0.998	0.329	1.944	0.992	0.429	1.856	0.991
		λ	0.115	0.165	0.979	0.083	0.130	0.973	0.056	0.099	0.988
		κ	0.087	0.112	0.970	0.065	0.081	0.948	0.040	0.054	0.953
	MH	β_1	0.299	0.356	0.927	0.204	0.250	0.923	0.135	0.154	0.881
		β_2	0.254	0.295	0.938	0.169	0.208	0.921	0.110	0.129	0.902
		β_3	0.043	0.052	0.941	0.029	0.036	0.916	0.020	0.023	0.901
		α	0.430	1.846	0.993	0.545	1.659	0.992	0.891	1.262	0.870
		λ	0.116	0.162	0.960	0.088	0.124	0.965	0.068	0.083	0.928
		κ	0.088	0.111	0.964	0.066	0.079	0.928	0.042	0.050	0.911
m_3	HMC	β_1	0.298	0.364	0.943	0.191	0.256	0.958	0.138	0.162	0.934
		β_2	0.239	0.300	0.947	0.162	0.211	0.963	0.110	0.133	0.939
		β_3	0.040	0.052	0.942	0.027	0.036	0.954	0.019	0.023	0.955
		α	0.115	0.802	0.993	0.155	0.768	0.998	0.207	0.683	0.991
		λ	0.182	0.289	0.976	0.148	0.232	0.984	0.109	0.183	0.997
		κ	0.085	0.113	0.969	0.063	0.082	0.955	0.041	0.056	0.972
	MH	β_1	0.308	0.348	0.899	0.205	0.246	0.928	0.144	0.153	0.864
		β_2	0.244	0.289	0.937	0.167	0.206	0.933	0.115	0.127	0.903
		β_3	0.041	0.051	0.925	0.028	0.035	0.948	0.020	0.022	0.907
		α	0.190	0.716	0.995	0.251	0.646	0.983	0.377	0.486	0.843
		λ	0.197	0.278	0.962	0.164	0.212	0.944	0.134	0.146	0.858
		κ	0.086	0.111	0.943	0.066	0.079	0.939	0.045	0.051	0.891
m_4	HMC	β_1	0.280	0.363	0.947	0.204	0.256	0.941	0.134	0.161	0.938
		β_2	0.242	0.299	0.928	0.176	0.212	0.929	0.113	0.133	0.921
		β_3	0.043	0.052	0.929	0.029	0.036	0.952	0.019	0.023	0.957
		α	0.125	0.777	0.991	0.158	0.759	0.996	0.206	0.681	0.994
		λ	0.123	0.188	0.977	0.085	0.156	0.981	0.068	0.126	0.991
		κ	0.090	0.113	0.960	0.060	0.082	0.961	0.039	0.056	0.966
	MH	β_1	0.289	0.351	0.937	0.210	0.244	0.909	0.137	0.151	0.894
		β_2	0.248	0.291	0.916	0.178	0.204	0.898	0.114	0.126	0.885
		β_3	0.043	0.051	0.918	0.030	0.035	0.951	0.019	0.022	0.911
		α	0.185	0.704	0.994	0.246	0.632	0.988	0.313	0.489	0.897
		λ	0.128	0.181	0.970	0.098	0.145	0.961	0.086	0.105	0.922
		κ	0.091	0.112	0.957	0.061	0.080	0.954	0.041	0.052	0.926

The Stan code implementing the proposed BTcr model, used in both the simulation study and the data applications, is available at `https://github.com/mpereira-ship-it/BTcr-stan`.

3.2. Applications

In this section, we illustrate the practical utility of the proposed BTcr model through two real-world applications. The first application uses the well-known melanoma dataset, which has been extensively employed in survival analysis studies and contains key prognostic variables such as survival time, ulceration status, and tumor thickness [36, 37]. The second application focuses on a cardiovascular disease dataset, enabling the assessment of the effects of comorbidities and other risk factors on patient survival. These applications highlight the model's flexibility and interpretability in capturing complex survival dynamics across diverse biomedical contexts.

3.2.1. Melanoma dataset

The melanoma dataset, available in the `timereg` package in R [38], originates from a Danish clinical study of patients who underwent surgery for malignant melanoma [39]. It has become a standard benchmark in survival analysis due to its well-structured format, thoroughly documented clinical covariates, and the presence of right-censored observations, which facilitate the evaluation and comparison of both parametric and semiparametric survival models. The key prognostic variables (survival time, ulceration status, and tumor thickness) have been consistently identified as important predictors of melanoma outcomes [37].

Table 2. Posterior mean estimates (SD) for the melanoma dataset from R. Convergence diagnostics ($\hat{R}$) ranged between 0.9998 and 1.0245.

Parameter	**BTcr**	**Bellcr**	**Berncr**	**Pocr**
$\beta_{(Intercept)}$	1.6060 (0.5508)	1.5922 (0.5749)	1.9688 (0.5263)	1.5108 (0.7021)
β_{ulcer}	−1.4372 (0.4240)	−1.4388 (0.4385)	−1.4840 (0.6741)	−1.5918 (0.6899)
β_{thick}	−0.0022 (0.0027)	−0.0024 (0.0041)	−0.0047 (0.0046)	−0.0046 (0.0096)
κ	1.6548 (0.2468)	1.6427 (0.2473)	1.3704 (0.2262)	1.5132 (0.2631)
λ	−3.3253 (0.4988)	−3.3072 (0.5438)	−2.5028 (0.3023)	−3.1889 (0.7071)
α	1.1490 (0.8834)	—	—	—
LOOIC	423.5	424.1	434.6	428.3

Table 2 and Figure 1 jointly summarize the comparison of candidate models based on leave-one-out (LOO) cross-validation metrics and expected log pointwise predictive density (ELPD) differences. The **BellTouch** model consistently demonstrates the best predictive performance, achieving the lowest LOOIC (423.5) and the smallest ELPD difference, which is closest to the reference value (zero). The Bellcr model shows very similar results, with a slightly higher LOOIC and marginally lower ELPD, indicating comparable fit quality. In contrast, the **Pocr** and **Berncr** models exhibit progressively larger ELPD differences and higher LOOIC values, reflecting weaker predictive performance relative to the reference. The error bars in Figure 1 represent the standard errors of the ELPD differences, highlighting

the uncertainty in the estimates. While the first two models differ only slightly, a marked deterioration is observed for **Pocr** and, especially, for **Berncr**, which exhibits the poorest overall fit. Overall, these results support selecting the BTcr specification as the most suitable model for the melanoma dataset, achieving the most reliable predictive performance among the evaluated candidates. Figure 2 presents the QQ-plot of the quantile residuals, suggesting that they follow a standard normal distribution; thus, the BTcr model is appropriate for this dataset. Finally, Figure 3 presents the estimated survival function by ulceration status for patients with a tumor thickness of 1.94 cm.

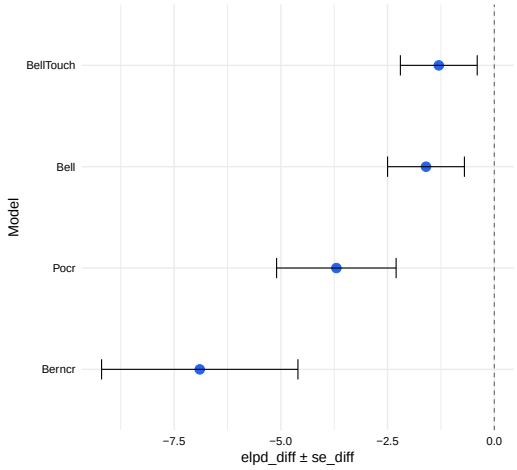

Figure 1. Expected log predictive density differences (elpd_diff) for four models relative to the best model, BTcr. Error bars indicate standard errors.

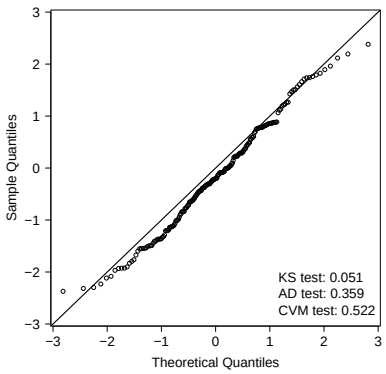

Figure 2. QQ-plot of quantile residuals for the melanoma dataset based on the BTcr model. Also presented are the p-values for the normality tests referred to.

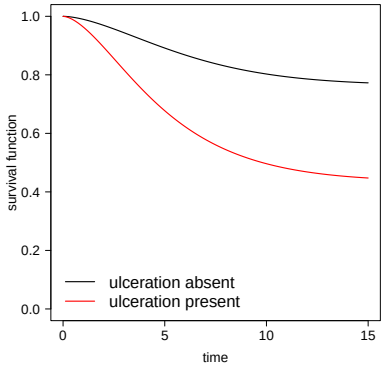

Figure 3. Estimated survival functions for different profiles of ulceration and a thickness of 1.94 cm.

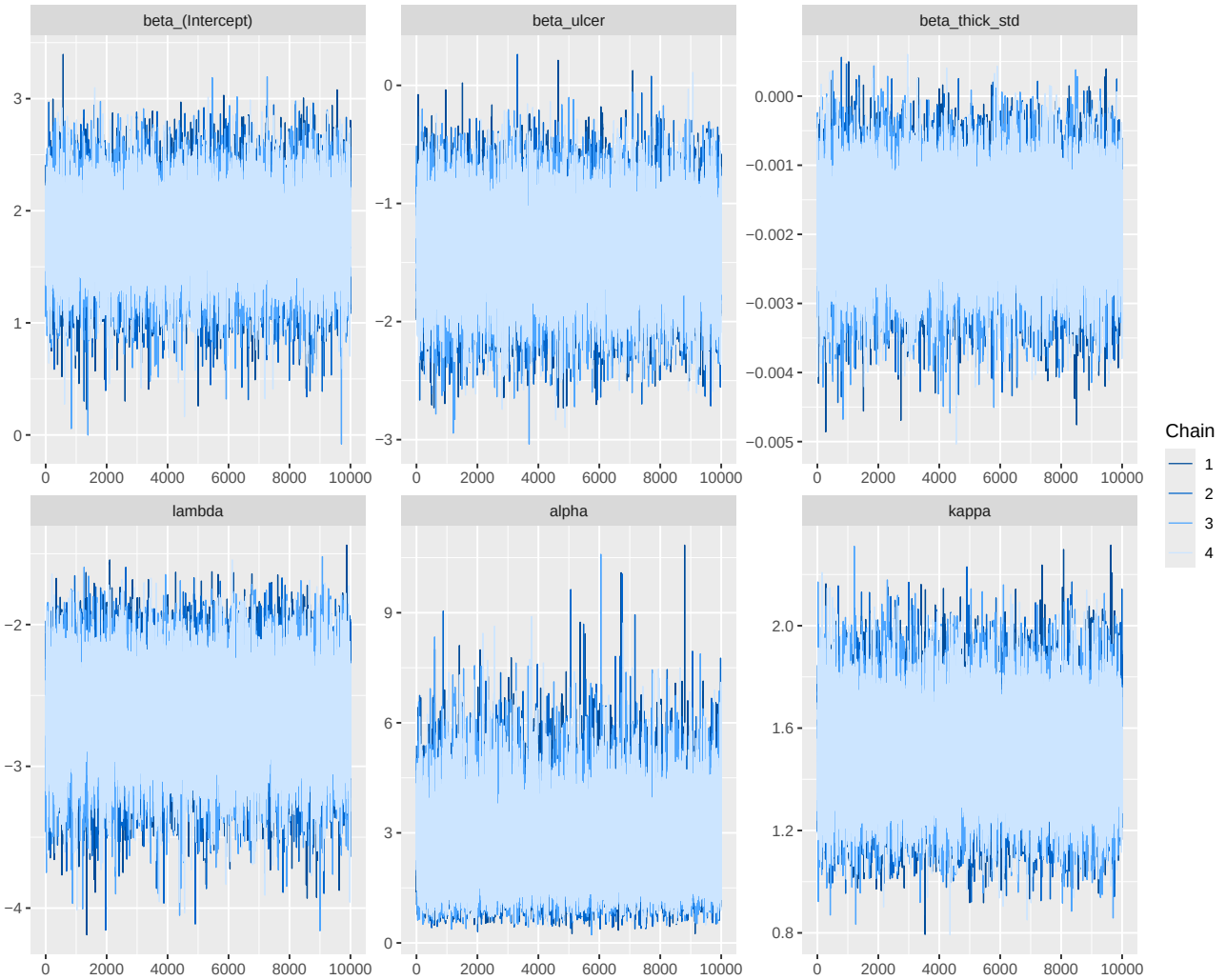

Figure 4. Trace plots of the HMC posterior samples for the BTcr model parameters in the melanoma dataset.

Trace plots for all BTcr parameters under the HMC method are shown in Figure 4 and display good

mixing across chains, with no visible non-stationarities.

To assess prior sensitivity for the BTcr model in this application, we considered three gamma priors for both the mixing parameter α and the Weibull rate parameter, denoted weak, mid, and tight, corresponding to Ga(1, 1), Ga(2, 1), and Ga(5, 2), respectively.

Table 3. LOO comparison of BTcr priors (ELPD differences) for the melanoma dataset.

Prior	elpd_diff	se_diff
Weak	0.0	0.0
Mid	-0.2	0.3
Tight	-0.9	1.0

The predictive performance of the BTcr model is essentially unchanged across the three prior specifications considered, with ELPD differences smaller than one standard error (Table 3).

3.2.2. Cardiovascular disease

We consider an application in cardiovascular disease, specifically in patients with ST-elevation myocardial infarction (STEMI). In this context, the prognostic value of apelin-12 has been investigated in a prospective observational study that included patients across different renal function strata [21, 22]. Modeling survival in this setting enables the identification of distinct risk patterns and potential cure rates, providing relevant information for prognostic stratification and informed clinical decision-making. The data used for this analysis were obtained from the study by Yang et al. [21], which included variables such as pre-existing cardiovascular disease, diabetes, hypnotic use, and smoking status. Incorporating these factors enables the construction of models that better reflect the characteristics of the study population, thereby improving risk prediction and subgroup identification with different survival trajectories. Figure 5 presents the Kaplan-Meier (KM) estimator for each covariate. Note that cardiovascular disease, hypnotika, and smoking are risk factors, whereas diabetes is a protective factor.

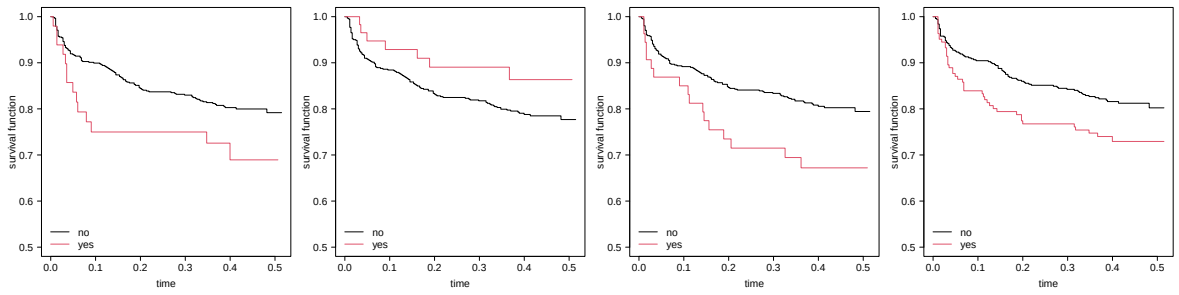

(a) cardiovascular **(b)** diabetes **(c)** hypnotika **(d)** smoking

Figure 5. Kaplan-Meier estimators for different covariates in cardiovascular disease dataset.

Table 4. Posterior mean estimates (SD) and model comparison for the cardiovascular disease dataset. Convergence diagnostics ($\hat{R}$) ranged between 0.9999 and 1.0044.

Parameter	BTcr	Bellcr	Berncr	Pocr
$\beta_{(Intercept)}$	1.2009 (0.4508)	1.2061 (0.4833)	1.0507 (0.5705)	1.1199 (0.6582)
$\beta_{\text{cardiovascular}}$	−0.7328 (0.3771)	−0.7280 (0.3806)	−0.9106 (0.6808)	−0.7601 (0.4528)
β_{diabetes}	0.8073 (0.4467)	0.8001 (0.4413)	0.9620 (0.5790)	0.8427 (0.4794)
$\beta_{\text{hypnotika}}$	−0.6127 (0.3409)	−0.6200 (0.3409)	−0.8826 (0.6898)	−0.6838 (0.4139)
β_{smoking}	−0.4509 (0.2284)	−0.4520 (0.2405)	−0.5782 (0.5142)	−0.4788 (0.2952)
k	0.8546 (0.0944)	0.8516 (0.0921)	0.7761 (0.1049)	0.8201 (0.0975)
λ	1.0840 (0.6113)	1.1165 (0.6124)	1.0214 (0.6570)	1.0724 (0.7159)
α	1.1026 (0.9494)	—	—	—
LOOIC	335.3	337.3	342.2	339.2

Table 4 presents the posterior mean estimates and standard deviations for all model parameters across the four candidate models, along with the leave-one-out information criterion (LOOIC) for model comparison. The BTcr model exhibits a slightly lower LOOIC (335.3) than the other models, suggesting superior predictive performance. Estimated regression coefficients indicate consistent effects across models: for instance, cardiovascular disease and smoking are associated with decreased survival probability, whereas diabetes shows a positive association in this dataset.

Figure 6 illustrates the expected log predictive density differences (elpd_diff) for the four models relative to the best-performing model, BTcr. As expected, BTcr has an elpd_diff of 0, indicating the highest predictive accuracy, while all other models have negative values. Bellcr performs similarly to BTcr, whereas **Pocr** and **Berncr** show larger negative deviations, reflecting lower predictive performance. Error bars correspond to the standard errors of the differences, highlighting the uncertainty in the estimates.

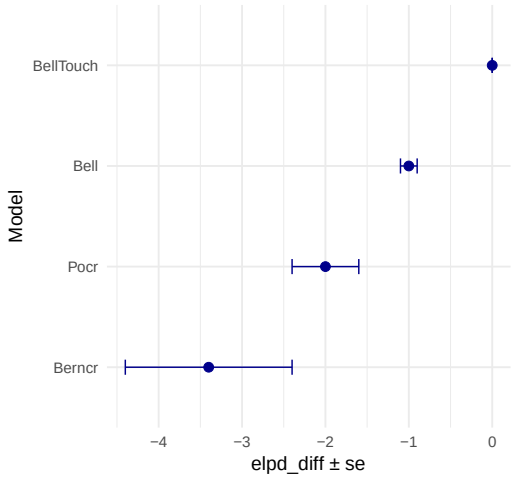

Figure 6. Expected log predictive density differences (elpd_diff) for the four models relative to BTcr. Error bars indicate standard errors.

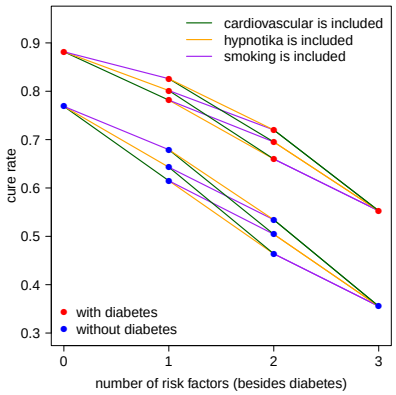

Figure 7. Estimated cure rates for different patient profiles based on cardiovascular disease, diabetes, hypnotic use, and smoking status.

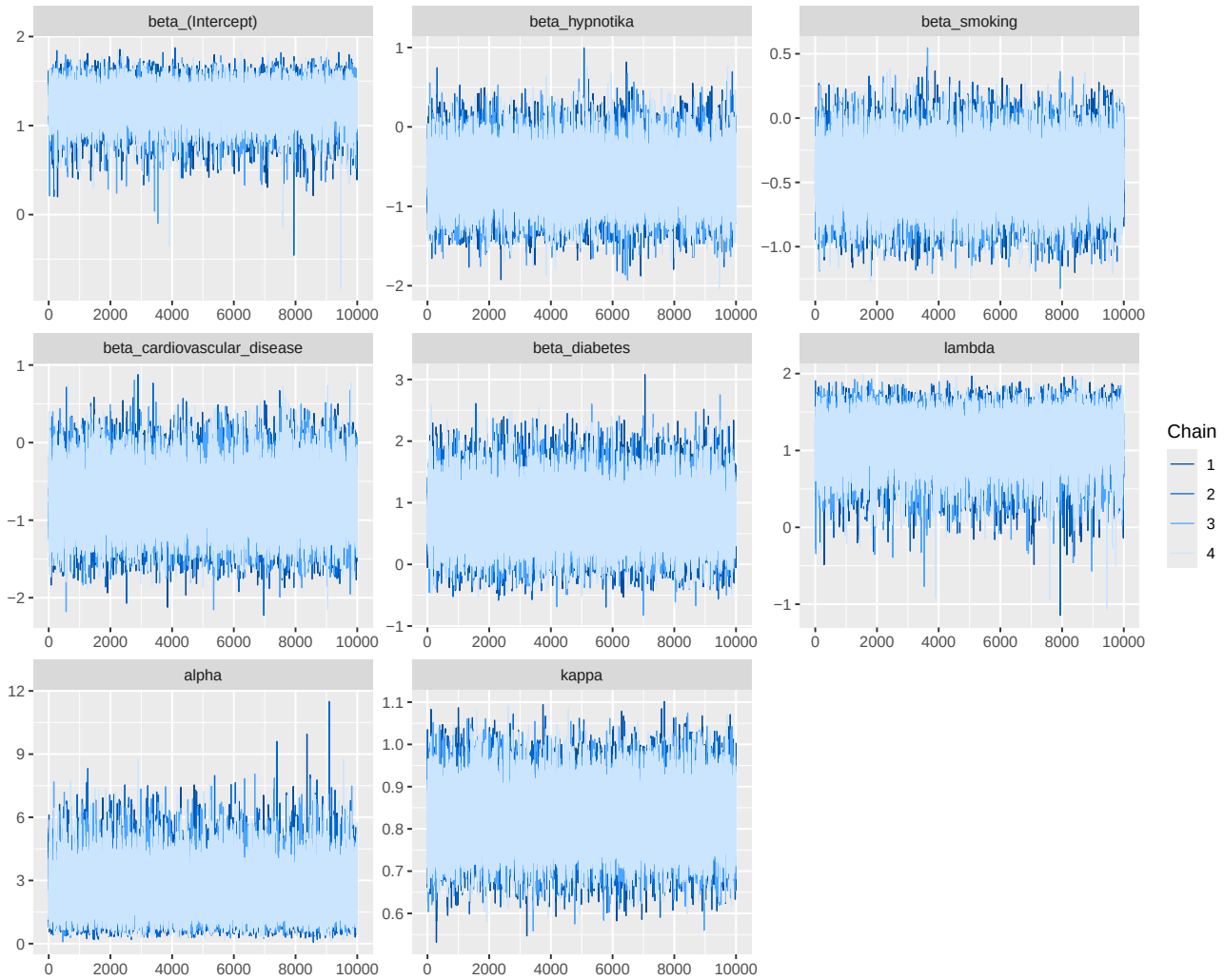

Figure 8. Trace plots of the HMC posterior samples for the BTcr model parameters in the cardiovascular disease dataset.

Figure 7 presents the estimated cure rates stratified by diabetes status and the presence of cardiovascular disease, hypnotic use, and smoking. A clear cumulative risk pattern is observed: as the number of risk factors increases, the probability of being cure decreases. Interestingly, the model indicates slightly higher cure probabilities for diabetic patients compared to non-diabetic patients, suggesting a nuanced effect of diabetes in this dataset.

Figure 8 presents trace plots of the HMC posterior samples for the BTcr parameters in the cardiovascular dataset; the chains mix well, and standard convergence diagnostics are satisfactory.

A similar pattern is observed when varying the priors on α and λ in the cardiovascular dataset: ELPD differences between weak, mid, and tight priors are negligible (Table 5), so the main conclusions do not depend on the specific prior choice.

Table 5. LOO comparison of BTcr priors (ELPD differences) for the cardiovascular disease dataset.

Prior	elpd_diff	se_diff
Weak	0.0	0.0
Mid	-0.1	0.2
Tight	-0.1	0.2

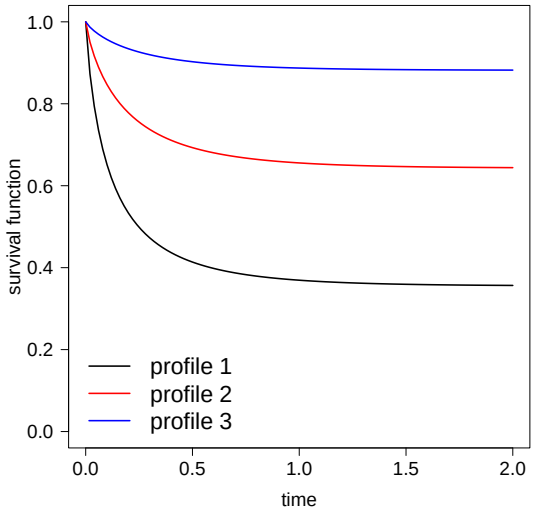

Figure 9. Estimated survival functions for three representative profiles: Profile 1 – cardiovascular: yes, diabetes: no, hypnotics: yes, smoking: yes; Profile 2 – cardiovascular: no, diabetes: no, hypnotics: yes, smoking: no; Profile 3 – cardiovascular: no, diabetes: yes, hypnotics: no, smoking: no.

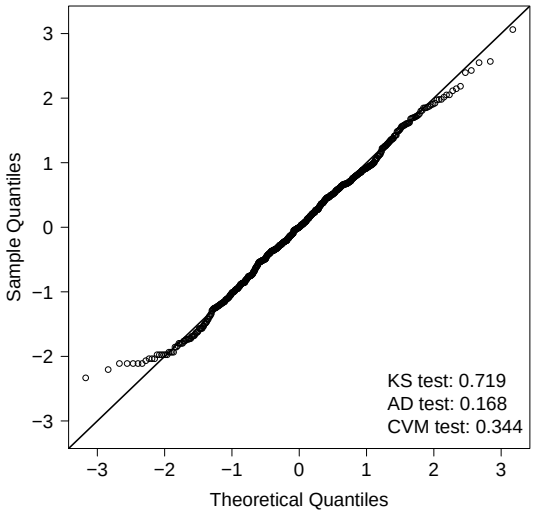

Figure 10. QQ-plot of quantile residuals for the cardiovascular disease dataset based on the BTcr model.

Figure 9 presents the estimated survival curves for three representative patient profiles. Profiles with multiple risk factors (cardiovascular disease, smoking, hypnotic use) exhibit lower survival probabilities over time. In contrast, patients with diabetes but without additional risk factors display more favorable survival trajectories, consistent with the cure rate estimates.

Finally, Figure 10 displays QQ-plots of the quantile residuals from the BTcr model, indicating adequate model fit to the cardiovascular disease data.

4. Final discussion

A new cure rate model was proposed in this study, in which the number of competing causes followed the Bell–Touchard distribution. The model's main mathematical properties were derived, and a Bayesian inference approach was implemented using the Hamiltonian Monte Carlo method. A simulation study was conducted for sample sizes $n = 200, 400$, and 1000, confirming the good performance and stability of the parameter estimates as the sample size increased. The proposed model was applied to two real datasets. The first was the well-known melanoma dataset from the timereg R package, where the Bell–Touchard cure model outperformed the alternative models. The second application involved a cardiovascular disease dataset, in which the proposed model also exhibited superior fit and interpretability. In the cardiovascular application, patients with diabetes showed higher estimated cure and survival probabilities than non-diabetic individuals. This finding may be explained by what has been termed "reverse epidemiology" (the obesity paradox) and by differences in clinical management and early intervention. Several studies have reported that patients with heart failure or other chronic cardiovascular conditions who are overweight or diabetic may experience better survival outcomes, possibly due to greater metabolic reserves, reduced frailty, or more frequent medical monitoring and treatment optimization (see, e.g., [40, 41]). Thus, this apparent paradox may reflect the benefits of intensified management among diabetic patients rather than a protective effect of the disease itself. In summary, the proposed Bell–Touchard cure rate model represents a flexible and robust alternative for modeling survival data with a cured fraction. Its

performance in both simulated and real datasets suggests it can capture complex survival dynamics more effectively than classical competing-risk cure models, offering valuable potential for biomedical and epidemiological applications.

Of course, we cannot claim that the cure model based on the Bell-Touchard distribution is better than everything proposed in the literature on cure fraction, since it is merely another alternative that does not include the more traditional models as special cases.

Finally, further research building on this work could focus on extending the model to account for random effects or measurement errors in the context of variables. Alternatively, the distribution of susceptible individuals, as described in Remark 1, could be further characterized. Lastly, the model could also be extended to accommodate different censoring schemes.

Author contributions

Manuel J. P. Barahona: Conceptualization, methodology, formal analysis, writing—original draft preparation, writing—review and editing; Yolanda M. Gómez: Conceptualization, methodology, formal analysis, writing—review and editing; Diego I. Gallardo: Conceptualization, methodology, formal analysis, writing—review and editing. Barahona, Gómez, and Gallardo contributed equally. All authors approved the final manuscript and are accountable for all aspects of the work.

Use of Generative-AI tools declaration

The authors declare they have not used Artificial Intelligence (AI) tools in the creation of this article.

Acknowledgments

D.I.G. gratefully acknowledges the DICREA - REGULAR project RE2432703 from the University of Bío-Bío for partially funding this work.

Conflict of interest

The authors declare no conflicts of interest.

References

1. J. W. Boag, Maximum Likelihood Estimates of the Proportion of Patients Cured by Cancer Therapy, *J. R. Stat. Soc. Ser. B*, **11** (1949), 15–53. https://doi.org/10.1111/j.2517-6161.1949.tb00020.x
2. J. Berkson, R. P. Gage, Survival curve for cancer patients following treatment, *J. Amer. Stat. Assoc.*, **47** (1952), 501–515. https://doi.org/10.1080/01621459.1952.10501187
3. M.-H. Chen, J. G. Ibrahim, D. Sinha, A new Bayesian model for survival data with a surviving fraction, *J. Amer. Stat. Assoc.*, **94** (1999), 909–919. https://doi.org/10.1080/01621459.1999.10474196

4. J. Rodrigues, V. G. Cancho, M. De Castro, N. Louzada-Neto, On the unification of the long-term survival models, *Stat. Prob. Lett.*, **79** (2009), 753–759. https://doi.org/10.1016/j.spl.2008.10.029

5. J. Rodrigues, M. de Castro, N. Balakrishnan, V. G. Cancho, COM–Poisson cure rate survival models and an application to a cutaneous melanoma data, *J. Stat. Plan. Infer.*, **139** (2009), 3605–3611. https://doi.org/10.1016/j.jspi.2009.04.014

6. V. G. Cancho, E. M. M. Ortega, L. de Oliveira, The power series cure rate model: An application to a cutaneous melanoma data, *Commun. Stat. Simul. Comput.*, **42** (2013), 586–602. https://doi.org/10.1080/03610918.2011.639971

7. D. I. Gallardo, H. W. Gómez, H. Bolfarine, A new cure rate model based on the Yule-Simon distribution with application to a melanoma data set, *J. Appl. Stat.*, **44** (2017), 1153–1164. https://doi.org/10.1080/02664763.2016.1194385

8. D. I. Gallardo, Y. M. Gómez, M.De Castro, A cure rate model based on the polylogarithm distribution, *J. Stat. Comput. Simul.*, **88** (2018), 2137–2149. https://doi.org/10.1080/00949655.2018.1451850

9. D. I. Gallardo, Y. M. Gómez, H.W. Gómez, M. De Castro, On the use of the modified power series family of distributions in a cure rate model context, *Stat. Methods Med. Res.*, **29** (2020), 1831–1845. https://doi.org/10.1177/0962280219876962

10. V. G. Cancho, M. A. C. Macera, A. K. Suzuki, F. Louzada, K. E. C. Zavaleta, A new long-term survival model with dispersion induced by discrete frailty, *Lifetime Data Anal.*, **26** (2020), 221–244. https://doi.org/10.1007/s10985-019-09472-2

11. J. Leão, M. Bourguignon, D. I. Gallardo, G. Rocha, V. Tomazella, A new cure rate model with flexible competing causes with applications to melanoma and transplantation data, *Stat. Med.*, **39** (2020), 3272–3284. https://doi.org/10.1002/sim.8664

12. H. C. Cavenague, F. Louzada, P. L. Ramos, M. R. de Oliveira Jr., G. da Silva, A Bayesian approach for the zero-inflated cure model: an application in a Brazilian invasive cervical cancer database, *J. Appl. Stat.*, **49** (2022), 3178–3194. https://doi.org/10.1080/02664763.2021.1933923

13. M. Santos-Neto, Y. M. Gómez, D. I. Gallardo, E. G. Costa, Bayesian modeling for a new cure rate model based on the Nielsen distribution, *Braz. J. Probab. Stat.*, **36** (2022), 807–820. https://doi.org/10.1214/22-BJPS557

14. Y. M. Gómez, D. I. Gallardo, M. Bourguignon, E. Bertolli, V. F. Calsavara, A general class of promotion time cure rate models with a new biological interpretation, *Lifetime Data Anal.*, **29** (2023), 66–86. https://doi.org/10.1007/s10985-022-09575-3

15. V. G. Cancho, M. M. Sacramento, E. M. M. Ortega, T. E. N. T.De Moraes, G. M. Cordeiro, A Bayesian cure rate regression model using Hamiltonian Monte Carlo methods, *Commun. Stat. Simul. Comput.*, **54** (2024), 4030–4047. https://doi.org/10.1080/03610918.2024.2370985

16. J. Rodrigues, V. G. Cancho, N. Balakrishnan, A. Suzuki, A Bayesian destructive generalized Waring regression cure model with a variance decomposition and application in colorectal cancer data, *J. Stat. Comput. Simul.*, **94** (2024), 3111–3130. https://doi.org/10.1080/00949655.2024.2368887

17. D. I. Gallardo, M. Brandão, J. Leão, M. Bourguignon, V. Calsavara, A New Mixture Model With Cure Rate Applied to Breast Cancer Data, *Biome. J.*, **66** (2024), e202300257. https://doi.org/10.1002/bimj.202300257

18. F. Louzada, P. L. Ramos, H. C. C. De Souza, L. Oyeneyin, G. S. C. Perdoná, On the unification of zero-adjusted cure survival models, *Commun. Stat. Simul. Comput.* 2025, 1–16. https://doi.org/10.1080/03610918.2025.2496297

19. F. Castellares, A. J. Lemonte, G. Moreno-Arenas, The Bell–Touchard discrete distribution: Properties and applications, *Commun. Stat. Theory Methods*, **49** (2020), 4834–4852. https://doi.org/10.1080/03610926.2019.1609515

20. D. I. Gallardo, M. De Castro, H.W. Gómez, An Alternative Promotion Time Cure Model with Overdispersed Number of Competing Causes: An Application to Melanoma Data, *Mathematics*, **9** (2021), 1815. https://doi.org/10.3390/math9151815

21. L. Yang, T. Zheng, H. Wu, W. Xin, X. Mou, H. Lin, Data from: Predictive value of apelin-12 in ST-elevation myocardial infarction patients with different renal function: A prospective observational study, Dryad, 2017. https://doi.org/10.5061/dryad.pf56m

22. L. Yang, T. Zheng, H. Wu, W. Xin, X. Mou, H. Lin, Predictive value of apelin-12 in patients with ST-elevation myocardial infarction with different renal function: A prospective observational study, *BMJ Open*, **7** (2017), e018595. https://doi.org/10.1136/bmjopen-2017-018595

23. M. De Castro, V. G. Cancho, J. Rodrigues, A Bayesian long-term survival model parametrized in the cured fraction, *Biom. J.: J. Math. Methods Biosci.*, **15** (2009), 433–454. https://doi.org/10.1002/bimj.200800199

24. V. G. Cancho, J. Rodrigues, M. De Castro, A flexible model for survival data with a cure rate: A Bayesian approach, *J. Appl. Stat.*, **38** (2011), 57–70. https://doi.org/10.1080/02664760903254052

25. V. G. Cancho, M. De Castro, J. Rodrigues, A Bayesian analysis of the Conway–Maxwell–Poisson cure rate model, *Stat. Pap.*, **53** (2012), 165–176. https://doi.org/10.1007/s00362-010-0326-5

26. J. Rodrigues, V. G. Cancho, M. De Castro, N. Balakrishnan, A Bayesian destructive weighted Poisson cure rate model and an application to a cutaneous melanoma data, *Stat. Methods Med. Res.*, **21** (2012), 585–597. https://doi.org/10.1177/0962280210391443

27. A. K. Suzuki, V. G. Cancho, F. Louzada, The Poisson–Inverse-Gaussian regression model with cure rate: a Bayesian approach and its case influence diagnostics, *Stat. Pap.*, **57** (2016), 133–159. https://doi.org/10.1007/s00362-014-0649-8

28. B. Yiqi, V. G. Cancho, F. Louzada, On the Bayesian estimation and influence diagnostics for the Weibull-Negative-Binomial regression model with cure rate under latent failure causes, *Commun. Stat. Theory Methods*, **46** (2017), 1462–1489. https://doi.org/10.1080/03610926.2015.1019150

29. A. Xu, W. Wang, Recursive Bayesian prediction of remaining useful life for gamma degradation process under conjugate priors, *Scand. J. Stat.*, **53** (2025), 175–206. https://doi.org/10.1111/sjos.70031

30. A. Xu, J. Wang, D. Zhu, Z. Chen, Y. Wang, A robust Bayesian framework for degra- dation state identification in the presence of outliers, *Nav. Res. Log.*, 2025, 1–19. https://doi.org/10.1002/nav.70033

31. A. D. Tsodikov, J. G. Ibrahim, A. Y. Yakovlev, Estimating cure rates from survival data: An alternative to two-component mixture models, *J. Amer. Stat. Assoc.*, **98** (2003), 1063–1078. https://doi.org/10.1198/016214503000000001007

32. L. Hanin, L. Huang, Identifiability of cure models revisited, *J. Multivar. Anal.*, **130** (2014), 261–274.

33. M. D. Hoffman, A. Gelman, The No-U-Turn Sampler: Adaptively Setting Path Lengths in Hamiltonian Monte Carlo, *J. Mach. Learn. Res.*, **15** (2014), 1593–1623.

34. A. Vehtari, A. Gelman, J. Gabry, Practical Bayesian model evaluation using leave-one-out cross-validation and WAIC, *Stat. Comput.*, **27** (2017), 1413–1432. https://doi.org/10.1007/s11222-016-9696-4

35. A. Vehtari, D. Simpson, A. Gelman, Y. Yao, J. Gabry, Pareto smoothed importance sampling, *J. Mach. Learn. Res.*, **25** (2024), 1–58.

36. P. K. Andersen, O. Borgan, R. D. Gill, N. Keiding, *Statistical Models Based on Counting Processes*, New York: Springer, 1993. https://doi.org/10.1007/978-1-4612-4348-9

37. C. M. Balch, J. E. Gershenwald, S. J. Soong, J. F. Thompson, D. S. Reintgen, A. J. Cochran, Final version of 2009 AJCC melanoma staging and classification, *J. Clin. Oncol.*, **27** (2009), 6199–6206. https://ascopubs.org/doi/abs/10.1200/JCO.2009.23.4799

38. T. Scheike, M. J. Zhang, Analyzing Competing Risk Data Using the R timereg Package, *J. Stat. Software*, **38** (2011), 1–15.

39. K. T. Drzewiecki, C. Ladefoged, H. E. Christensen, Biopsy and prognosis for cutaneous malignant melanoma in clinical stage I, *Scand. J. Plast. Reconstr. Surg.*, **14** (1980), 141–144. https://doi.org/10.3109/02844318009106699

40. A. L. Clark, G. C. Fonarow, T. B. Horwich, Obesity and the Obesity Paradox in Heart Failure, *Prog. Cardiovasc. Dis.*, **56** (2014), 409-414. https://doi.org/10.1016/j.pcad.2013.10.004

41. H. Fröhlich, A. Bossmeyer, S. Kazmi, K. M. Goode, S. Agewall, D. Atar, Glycaemic control and insulin therapy are significant confounders of the obesity paradox in patients with heart failure and diabetes mellitus, *Clin. Res. Cardiol.*, **113** (2024), 822–830. https://doi.org/10.1007/s00392-023-02268-3

AIMS Press